J Comp Physiol A (2016) 202:445–456
DOI 10.1007/s00359-016-1089-9

ORIGINAL PAPER

# Absence of gliosis in a teleost model of spinal cord regeneration

**Antonia G. Vitalo[1] · Ruxandra F. Sîrbulescu[1] · Iulian Ilieş[1] · Günther K. H. Zupanc[1]**

Received: 31 March 2016 / Revised: 28 April 2016 / Accepted: 29 April 2016 / Published online: 25 May 2016


**Abstract** Among the cellular processes that follow injury to the central nervous system, glial scar formation is thought to be one of the major factors that prevent regeneration. In regeneration-competent organisms, glial scar formation has been a matter of controversy. We addressed this issue by examining the glial population after spinal cord injury in a model of regeneration competency, the knifefish *Apteronotus leptorhynchus*. Analysis of spinal cord sections immunostained against the glial markers glial fibrillary acidic protein, vimentin, or chondroitin sulfate proteoglycan failed to produce any evidence for the formation of a glial scar in the area of the lesion at post-injury survival times ranging from 5 to 185 days. This result was independent of the lesion paradigm applied—amputation of the caudal part of the spinal cord or hemisection lesioning—and similar after examination of transverse and longitudinal sections. We hypothesize that the well-developed network of radial glia in both the intact and the injured spinal cord provides a support system for regeneration of tissue lost to injury. This glial network is likely also involved in the generation of new cells, as indicated by the large subset of glial fibrillary acidic protein-labeled glia that express the stem cell marker Sox2.

**Keywords** Gliosis · Spinal cord injury · Regeneration · Teleost fish · *Apteronotus leptorhynchus*

✉ Günther K. H. Zupanc
g.zupanc@neu.edu

[1] Laboratory of Neurobiology, Department of Biology, Northeastern University, 134 Mugar Life Sciences, 360 Huntington Avenue, Boston, MA 02115, USA

## Introduction

Spinal cord injury (SCI) is a devastating condition in non-regenerative organisms such as mammals. The initial lesion is characterized by local tissue disruption and necrosis, followed within hours by secondary phenomena, including ischemia, prolonged inflammation, and glial scar formation (Dusart and Schwab 1994; Fitch et al. 1999; Kwon et al. 2004). The glial scar creates an inhibitory environment in which axonal growth cones become dystrophic and retract, preventing successful regeneration (Horn et al. 2008; Rolls et al. 2009; Yuan and He 2013; Cregg et al. 2014). In stark contrast to mammals, regeneration-competent organisms such as teleost fish and urodele amphibians have the ability to regrow nervous tissue after spinal cord transection and even partial ablation [for reviews, see (Sîrbulescu and Zupanc 2011; Diaz Quiroz and Echeverri 2013; Lee-Liu et al. 2013)]. In teleosts, apoptosis (rather than necrosis), cell proliferation, and neuronal differentiation dominate after injury, and numerous molecular factors that promote regeneration have been identified in these organisms [for reviews, see (Sîrbulescu and Zupanc 2013; Zupanc and Sîrbulescu 2013)].

Reports vary on the extent of gliosis after central nervous system (CNS) injury in regeneration-competent vertebrates. Some studies have failed to find evidence for the formation of a glial scar in response to CNS lesions. For example, after application of stab wound lesions to the telencephalon of elasmobranchs, no significant astroglial reaction was found in the area surrounding the wound, as indicated by the absence of glial fibrillary acidic protein (GFAP)-positive cells (Kálmán et al. 2013). Other studies have uncovered the development

of an astrocytic response after CNS injuries. Following complete transection of the spinal cord in zebrafish, an astrocytic bridge is formed across the gap generated through the lesion (Goldshmit et al. 2012). This bridge is formed by astrocytes assuming an elongated bipolar morphology, and supports axonal elongation across the lesion site. By contrast, the glial scar found in mammals is composed of a dense plexus of interdigitated processes of glial cells with a stellate morphology that prevents the ingrowth of axons [for review, see (Sofroniew and Vinters 2010)]. In yet other regeneration-competent model systems, some form of glial scarring appears to accompany CNS injuries, however without impairing regeneration. In goldfish, reactive gliosis has been reported in an early study (Bernstein and Bernstein 1969), and more recent investigations confirmed the formation of a fibrous glial scar, containing collagen and laminin, following a thoracic or cervical crush or transection injury of the spinal cord (Takeda et al. 2007, 2015). In brown ghost knifefish, reactive gliosis has been reported after cerebellar lesions in the form of hypertrophied and displaced GFAP-expressing astrocytes (Clint and Zupanc 2001). In zebrafish, despite the possible occurrence of gliosis, neuronal regeneration and axonal regrowth through the fibrous glial scar can take place, and are complemented by functional recovery of behaviors associated with motor neuron regeneration after SCIs (Becker et al. 1997; Reimer et al. 2008).

In light of the controversy surrounding the formation and nature of a glial scar after spinal cord lesions in teleosts, in the present study we examined the cellular response of glia to SCI in one of the best characterized regeneration-competent model organisms, the brown ghost knifefish [for reviews, see (Sîrbulescu and Zupanc 2011, 2013; Zupanc and Sîrbulescu 2013)]. By employing two lesion paradigms—amputation of the caudal part of the spinal cord, and spinal cord hemisection—we found no evidence supporting the occurrence of glial scarring in this species.

## Materials and methods

### Animals

A total of 40 brown ghost knifefish (*Apteronotus leptorhynchus*; Gymnotiformes; Teleostei) with an average total length of 125 mm (range: 86–160 mm) and an average body mass of 5.3 g (range: 1.8–10.8 g) were used in this investigation. The gonadosomatic index averaged 0.17 % (range: 0.07–0.32 %) in males, and 2.56 % (range: 0.80–7.52 %) in females. Fish were supplied by tropical fish importers (East Coast Transhipping, Inc.) and housed in 40–300 L aquaria at temperatures of 26–28 °C and pH values of approximately 7.4, under a 12:12-h light/dark cycle.

### Tissue sampling

#### *Caudal amputation*

Under general anesthesia with 2 % ethyl carbamate (urethane; Fisher Scientific) in aquarium water and local anesthesia with 2 % lidocaine (Fisher Scientific), the caudal peduncle was amputated, removing approximately 10 % of the total body length of the fish.

#### *Hemisection*

The fish were anesthetized as described above, and 2–3 scales were removed from the lateral aspect of the caudal peduncle, approximately 1.5-cm rostral from the tip of the tail. A small incision was performed in the skin, exposing the spine, and after removing the bone with fine tweezers, the spinal cord was hemisectioned using fine iridectomy scissors.

#### *Perfusion and tissue sectioning*

After 0, 5, 7, 10, 20, 50, 100, or 185 days ($n$ = 2–6 fish per survival time), animals were deeply anesthetized using ethyl 3-aminobenzoate methanesulfonate (MS-222; Sigma Aldrich) dissolved in aquarium water, and perfused transcardially with heparinized saline solution, followed by 2 % freshly depolymerized paraformaldehyde (Fisher Scientific) in 0.1 M phosphate buffer, pH 7.4, for 30 min. The caudal-most 1 cm of the tail, including any regenerated tissue, was removed and post-fixed in 2 % paraformaldehyde for a minimum of 4 h, then cryoprotected overnight at 4 °C in 1 M sucrose in phosphate-buffered saline (PBS). Transverse and longitudinal sections were cut serially at a thickness of 16 µm, and mounted onto SuperFrost Plus Gold slides (Fisher Scientific).

### Immunohistochemistry

For immunohistochemical detection of antigens, sections were dried in a desiccator for 90 min at room temperature (RT) and rehydrated through three changes of PBS (pH 7.4). To permeabilize the tissue and block unspecific binding sites, sections were treated for 1 h at RT with PBS containing 1 % bovine serum albumin, 1 % teleostean gelatin, 3 % normal sheep serum, and 0.3 % Triton X-100 (all from Fisher Scientific). Sections were then incubated overnight at 4 °C with one of the following primary antibodies, diluted in blocking solution: monoclonal mouse anti-GFAP (clone G-A-5; 1:50;

Sigma Aldrich), polyclonal rabbit anti-GFAP (1:100; Sigma Aldrich), monoclonal mouse anti-vimentin (clone V9; 1:100; Sigma Aldrich), monoclonal mouse anti-chondroitin sulfate (clone CS-56; 1:50; Abcam), and polyclonal rabbit anti-Sox2 (1:50; Abcam). Unbound primary antibody was removed by 3 rinses for 5 min each in PBS. Sections were further incubated for 30 min at RT in blocking solution, as described above, except that normal goat serum was used instead of normal sheep serum. Antigenic sites were visualized by incubating the sections at RT for 90 min or at 4 °C overnight with the following corresponding secondary antibodies, diluted in blocking solution: Alexa Fluor 488-conjugated goat anti-rabbit IgG, Alexa Fluor 488-conjugated goat anti-mouse IgG, Alexa Fluor 546-conjugated goat anti-rabbit IgG, Alexa Fluor 546-conjugated goat anti-mouse IgG, Alexa Fluor 635-conjugated goat anti-mouse IgG (1:200; all from Life Technologies), or Cy3-conjugated goat anti-rabbit IgG (1:500; Jackson Immunoresearch). Sections were counterstained by incubation with 2 μg/ml of 4′, 6-diamidino-2-phenylindoledihydrochloride (DAPI; Sigma Aldrich) in PBS for 3 min at RT. The sections were washed 3 times for 7 min in PBS and embedded in polyvinyl alcohol containing *n*-propyl gallate.

### Antibody controls

Previous studies in the CNS of *A. leptorhynchus* demonstrated the specificity of the monoclonal mouse anti-GFAP antibody, the monoclonal mouse anti-vimentin antibody (Zupanc et al. 2012), and the rabbit anti-Sox2 antibody (Traniello et al. 2014). Double immunolabeling experiments using the monoclonal mouse anti-GFAP antibody and polyclonal rabbit anti-GFAP antibody showed a complete overlap of the labeling. For all antibodies used, negative controls, in which the primary antibody was omitted, were included.

### Microscopy

Images were acquired using a Zeiss Axioskop 20 epifluorescence microscope equipped with 20× and 40× objectives and an Axio-Cam MRc5 digital camera (both from Carl Zeiss), or a Zeiss LSM 710 laser scanning microscope (Carl Zeiss) equipped with 20×, 40× and 63× objectives. Epifluorescence images were taken at a resolution of 0.2 μm/pixel and an optical thickness of 16 μm using AxioVision (Carl Zeiss). Since they showed very high variability in fluorescence intensity when assessed under standard imaging settings, individual images were acquired at their automatically determined optimal exposure times. These ranged from 0.5 to 33 s across all examined sections, indicating an overall high dynamic range. Images were then linearly scaled using MATLAB (The MathWorks, Inc.) to a typical exposure time of 4.0 s for green fluorescence and 5.0 s for red fluorescence, resulting in effective dynamic ranges of 0–2040 and 0–2550, respectively.

Confocal images were taken at a resolution of 0.2–0.5 μm/pixel and an optical thickness of 2–5 μm using Zen (Carl Zeiss). Z-stacks were acquired at an offset of 0.9–2.5 μm per slice, and a total number of 9–35 optical slices per z-stack. For quantitative analysis, z-stacks were converted to single images by applying a maximum intensity projection, using ImageJ (National Institutes of Health). To correct for differences in intensity due to variations in label penetration and total optical thickness, confocal images of longitudinal sections were linearly scaled to an average background intensity of 90 (on a scale from 0 to 255) using MATLAB. Briefly, low-intensity regions (i.e., tissue areas without label) were identified through automatic image thresholding, and overall background levels were approximated through morphological image reconstruction. Each image was then rescaled such that the average background intensity within the examined tissue equaled the selected value (90). This scaling ensured that the strongest labeled regions attained intensities close or equal to the maximum (255) throughout all examined sections.

### Image analysis

For all microscopy images, regions of interest—including all spinal cord tissue but excluding the central canal—were outlined manually using ImageJ. For longitudinal sections, the region(s) of interest were divided into sub-regions of approximately 50 μm × 50 μm using MATLAB. To determine the positions of these sub-regions on the caudo-rostral axis, the medial line of the spinal cord was interpolated using a cubic spline, and the curve length between the caudal end of the cord and the projection onto this spline of each sub-region centroid was measured. For both transverse and longitudinal sections, GFAP and vimentin immunolabelings within the regions of interest were quantified in MATLAB using functions from the Image Processing Toolbox. Briefly, background levels were determined through image smoothing, followed by morphological image opening and morphological image closing for the high-noise epifluorescence images or, equivalently, watershed-based image segmentation and morphological image reconstruction for the low-noise confocal images. Pixels whose intensity exceeded the background levels by more than a predefined threshold, ranging between 5 and 150 as a function of background intensity for the high-dynamic-range epifluorescence images, and set to 20 for the standard-dynamic-range confocal images, were marked as foreground.

These threshold values were found to optimally distinguish between labeled and non-labeled structures during preliminary data analysis and corresponding MATLAB code development. The average immunolabeling density was calculated as the cumulative intensity of foreground pixels after background subtraction, divided by the total number of pixels in the analyzed region. Correspondingly, the average immunolabeling intensity was computed as the average intensity of foreground pixels after background subtraction.

### Data analysis

For statistical analysis of immunolabeling with glial markers, the examined portion of the spinal cord was divided along the caudo-rostral axis into 4-mm regions for transverse sections and 200-µm regions for longitudinal sections. Region indices were assigned in a caudo-rostral manner, with region 0 being centered on the injury site, regions with negative indices representing the regenerate, and regions with positive indices denoting progressively rostral levels of the non-regenerated spinal cord. Region indices for intact spinal cord samples collected from non-injured fish were assigned in a similar manner, with the caudal-most region being aligned with, and receiving the same index as, the caudal-most regenerate region at the longest survival times. Hypothesis testing was conducted using mixed-effects ANOVA models with type IV sum of squares. The post-injury survival time and the spinal cord region were included as between-subjects factors, while fish index or section index were included as nested random factors. For analysis of relative cell counts, a repeated measures ANOVA model with type III sum of squares was used. The experimental condition (tissue type and/or survival time) was included as a between-subjects factor, while cell type was included as a within-subjects factor. In

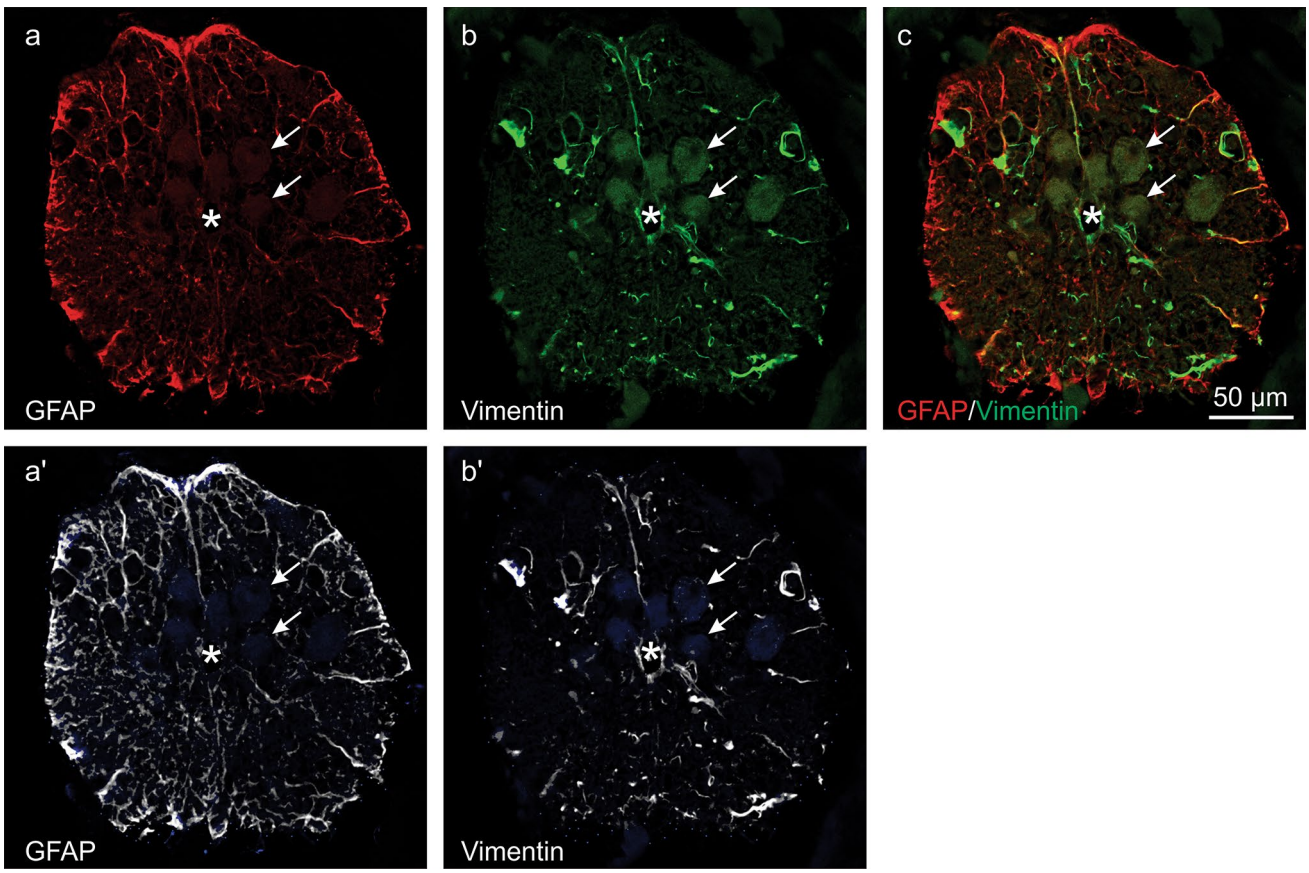


**Fig. 1** Detection of GFAP and vimentin immunopositive fibers in transverse spinal cord sections. **a–c** Confocal image showing GFAP (**a**) and vimentin (**b**) immunoreactivity in a representative transverse section collected from non-regenerated spinal cord. The *overlay* (**c**) indicates that, while both markers are mostly co-expressed, glial cells in certain areas express either vimentin or GFAP. The image represents a 2.3-µm-thick optical section. **a′–b′** Background levels (*blue*) were determined through image smoothing followed by morphological image opening. Pixels whose intensity exceeded the background levels by more than a predefined threshold were marked as foreground, and defined the immunolabeled fibers (*white*). Note that through this procedure autofluorescent structures, such as large electromotor neurons (*arrows*), were successfully excluded. The central canal is indicated by *asterisk* in each panel

all cases, post hoc multiple comparisons were performed using the Bonferroni method, and levels of statistical significance were adjusted accordingly. All reported descriptive statistics are estimated marginal means ± standard errors. All statistical analyses were conducted using SPSS (IBM Corporation).

## Results

### Absence of gliosis after spinal cord amputation

In order to assess possible changes in expression of classical glial markers after injury, transverse spinal cord sections were immunolabeled against GFAP and vimentin. Labeling patterns were examined in every fifth section of the caudal-most 1 cm of the spinal cord at 0, 5, 10, 20, 50, and 100 days after caudal amputation ($n = 3$ fish per time point). These tissue sections included the complete regenerated part as well as a portion of the non-regenerated tissue of the spinal cord. For statistical analysis, the examined sections were partitioned along the caudo-rostral axis into 4-mm regions. The intensity of the staining and the area of the central nervous tissue covered by immunopositive fibers were quantified in microscopy images as a measure of glial reactivity and hypertrophy (Fig. 1).

Analysis of the GFAP immunolabeling density did not reveal any significant effect of survival time ($F_{(5, 16.6)} = 0.57$, $p = 0.72$), nor any significant interaction between survival time and spinal cord region ($F_{(9, 28.5)} = 1.58$, $p = 0.17$). The analysis uncovered, however, a small, significant effect of spinal cord region ($F_{(3, 66.3)} = 3.45$, $p = 0.02$, $\eta^2 = 0.13$). Post hoc multiple comparisons indicated that the average GFAP density was significantly lower in the regenerated caudal region than near the injury site (7.1 vs. 10.0, $p = 0.03$), suggesting a reduced prevalence of mature glia in the newly generated tissue. No significant differences in GFAP labeling density

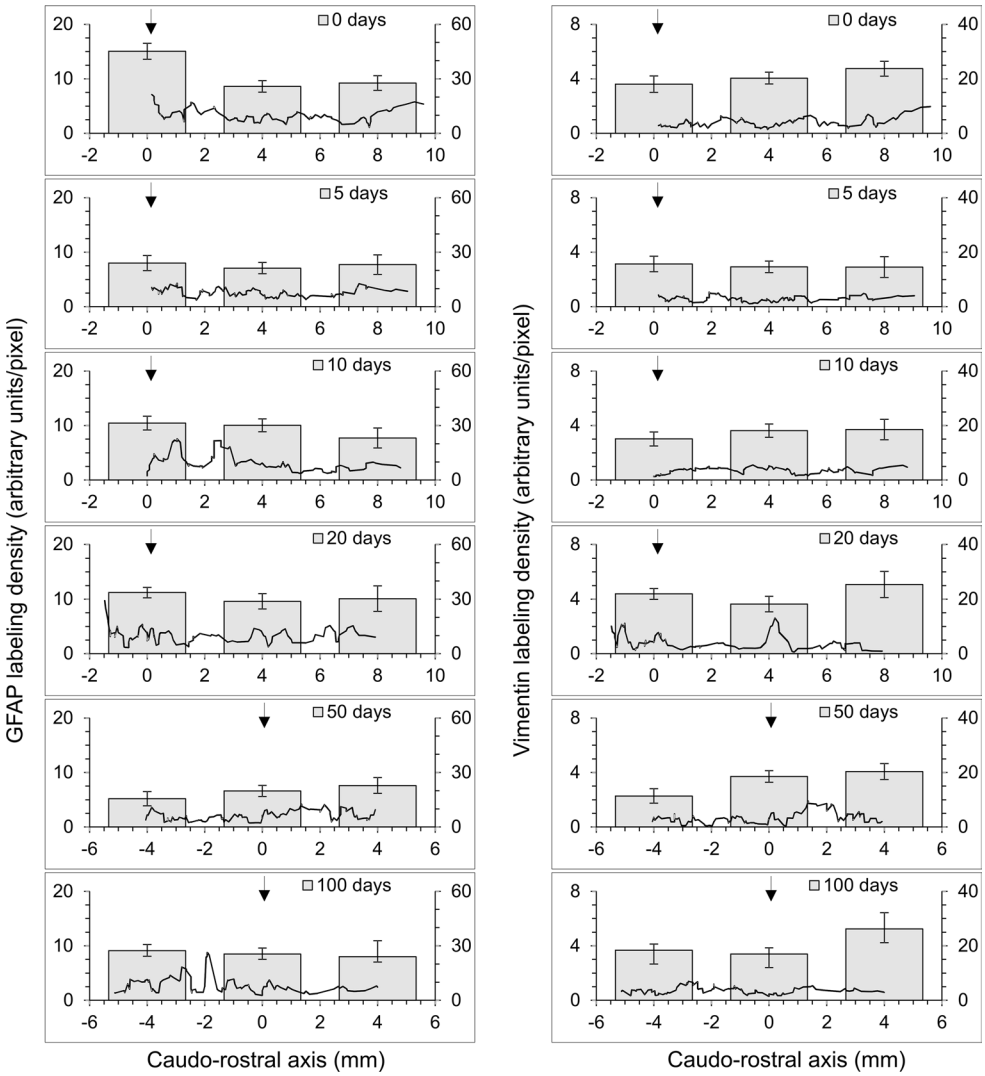


**Fig. 2** Quantification of GFAP and vimentin immunolabeling within the caudal-most 1 cm of the spinal cord at different post-amputation survival times. The average immunolabeling density was determined in transverse sections (24–44 sections per fish, 3 fish per time point) distributed uniformly throughout the examined spinal cord segment. For statistical analysis, sections were aligned on the caudo-rostral axis such that 0 corresponded to the injury site (*arrows*), and grouped into 4-mm bins centered at −4, 0, 4 and/or 8 (11–60 sections per bin per time point). *Columns* represent the corresponding estimated marginal means, and *error bars* denote their standard errors (*left y axis*). Overlaid traces represent 5-point moving averages of the density measurements of individual sections, pooled across fish (*right y axis*). Positive coordinates (right of the *arrow*) correspond to non-regenerated tissue, while negative coordinates (left of the *arrow*) denote regenerated tissue

were observed between any of the other spinal cord regions examined ($p > 0.46$), a pattern that was consistent across all time points (Fig. 2). The average intensity of immunolabeled GFAP fibers did not vary significantly with either survival time ($F_{(5,\ 16.7)} = 0.14$, $p = 0.98$), spinal cord region ($F_{(3,\ 36.7)} = 1.00$, $p = 0.40$), or their interaction ($F_{(9,\ 25.5)} = 0.47$, $p = 0.88$), suggesting that any observed differences in GFAP density arose from changes in the relative area covered by fibers instead.

Analysis of the vimentin immunolabeling density revealed no additional patterns (Fig. 2). Neither spinal cord region nor survival time had any significant effect on the labeling density ($F_{(3,\ 26.9)} = 0.64$, $p = 0.60$, and $F_{(5,\ 21.5)} = 0.32$, $p = 0.90$, respectively), and the same was true for their interaction ($F_{(9,\ 24.7)} = 0.18$, $p = 0.99$). As for GFAP, the average intensity of vimentin fibers did not vary significantly with spinal cord region ($F_{(3,\ 28.2)} = 0.62$, $p = 0.61$), survival time ($F_{(5,\ 14.1)} = 0.11$, $p = 0.99$), or their interaction ($F_{(9,\ 25.0)} = 0.32$, $p = 0.96$).

To further examine the expression of glial markers along the caudo-rostral axis of the spinal cord, we analyzed longitudinal sections of intact and regenerating tissue, at 0, 20, 50, and 185 days after caudal amputation ($n = 2$–6 fish per time point). Longitudinal sections were immunolabeled against GFAP (Fig. 3a–c) and vimentin (not shown); due to the high degree of expression similarity between the two markers, only the former was analyzed. GFAP labeling was quantified in tissue samples extending up to 2.5 mm on either side of the injury site, as well as in corresponding samples collected from the caudal region of intact spinal cords (Fig. 4). Sections were divided into a large number of small, roughly 50 µm × 50 µm regions of interest, thereby providing a 20-fold increase in caudo-rostral resolution as compared to the previous analysis on transverse sections. Results indicated that the average density of GFAP fibers did not vary significantly within this caudo-rostral range with either time point ($F_{(4,\ 19.5)} = 1.80$, $p = 0.17$), spinal cord region ($F_{(25,\ 215.9)} = 0.72$, $p = 0.83$), or their interaction ($F_{(58,\ 234.9)} = 0.89$, $p = 0.69$), confirming our initial findings. Similarly, there were no significant effects of time point ($F_{(4,\ 17.2)} = 0.30$, $p = 0.87$), spinal cord region ($F_{(25,\ 214.7)} = 0.98$, $p = 0.51$), or their interaction ($F_{(58,\ 236.8)} = 1.00$, $p = 0.48$) on GFAP labeling intensity. Since this analysis also included the caudal intact spinal cord, these results suggest that GFAP expression does not differ between regenerating and normally growing spinal cord tissue.

A major inhibitory component of the glial scar in the mammalian CNS is represented by chondroitin sulfate proteoglycans (CSPGs), extracellular matrix molecules secreted by reactive astrocytes at the site of the lesion (Yiu and He 2006). Here, we performed a qualitative immunohistochemical assessment of the changes in the expression of CSPGs at the injury site and neighboring regions in the *A. leptorhynchus* spinal cord at 0, 20, 50, and 185 days after caudal amputation. Our analysis indicated no differences in the CSPG immunolabeling at or around the lesion, at any time point examined (Figs. 3d–d", e–e"). This result was similar to the pattern observed after anti-GFAP immunostaining, and therefore no further quantitative analysis was carried out.

**Fig. 3** Absence of gliosis at the injury site after caudal spinal cord amputation. Composite tiled confocal images showing GFAP labeling in representative longitudinal sections collected immediately after amputation (**a**), 20 days post-amputation (**b**), and 50 days post-amputation (**c**). The spinal cord tissue, distinguished by its bright immunoreactivity against GFAP (*asterisk*), is surrounded by other types of tissue, some of which exhibit weak autofluorescence at 488 nm (*diamond*). **a** Maximum intensity projection of a series of 22 2.8-µm-thick confocal optical sections spanning a total of 61.6 µm. The image shows the distribution of GFAP-positive glia immediately after injury. The site of amputation is indicated by *arrow*. The non-regenerated tissue is to the right of the *arrow*. **b** Maximum intensity projection of a series of 19 2.5-µm-thick confocal optical sections spanning a total of 47.1 µm. At 20 days post-amputation, no visible increase in GFAP immunopositive fibers can be observed at the injury site (*arrow*). At this time point, over 1.5 mm of the caudal spinal cord has regenerated (left of the *arrow*). **c** Maximum intensity projection of a series of 30 2.5-µm-thick optical sections spanning a total of 74.4 µm. Similarly as at 20 days post-amputation, at 50 days no increase in GFAP immunoreactivity is evident at the injury site (*arrow*). **d**, **e** Magnified view of the spinal cord at the lesion site (*dashed line*), immunostained against CSPG and GFAP, at 20 days (**d**) and 185 days (**e**) after caudal amputation. The intensity of immunoreactivity against these two markers does not differ between regenerated (left of *dashed line*) and non-regenerated (right of *dashed line*) tissue, indicating the absence of local glial scar formation. Individual channels are shown in the panels below (**d′**, **d″**, **e′**, **e″**). Images are maximum intensity projections of series of 6 1.0-µm-thick confocal optical sections spanning a total of 5.8 µm (**d**, **d′**, **d″**), and 7 1.0-µm-thick confocal optical sections spanning a total of 6.8 µm (**e**, **e′**, **e″**)

## Absence of gliosis after spinal cord hemisection

To assess whether the observed absence of a glial scar formation was due to the type of SCI employed, an alternative experimental paradigm, lateral hemisection, was used instead of amputation. At 7 days post-lesion, spinal cord sections were immunolabeled against GFAP (Fig. 5) and vimentin (not shown), and evaluated for glial scar formation. No increase in either the number of glial cells or the area covered by glial processes, as indicated by the pattern and intensity of GFAP immunolabeling, was observed at the injury site, which was almost indistinguishable from the neighboring regions of the spinal cord.

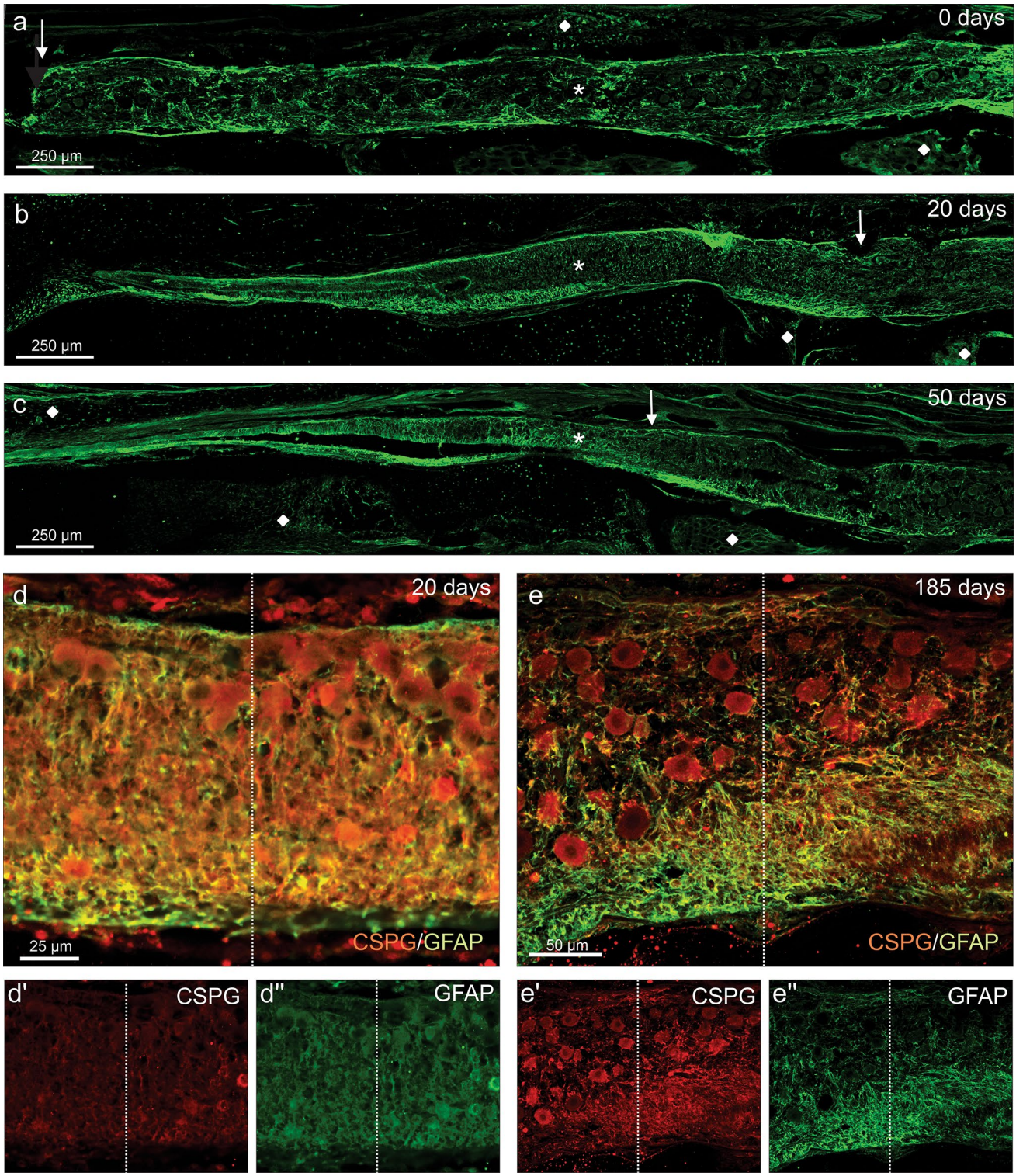
a
0 days
250 µm
b
20 days
250 µm
c
50 days
250 µm
d
20 days
25 µm
CSPG/GFAP
e
185 days
50 µm
CSPG/GFAP
d'
CSPG
d''
GFAP
e'
CSPG
e''
GFAP

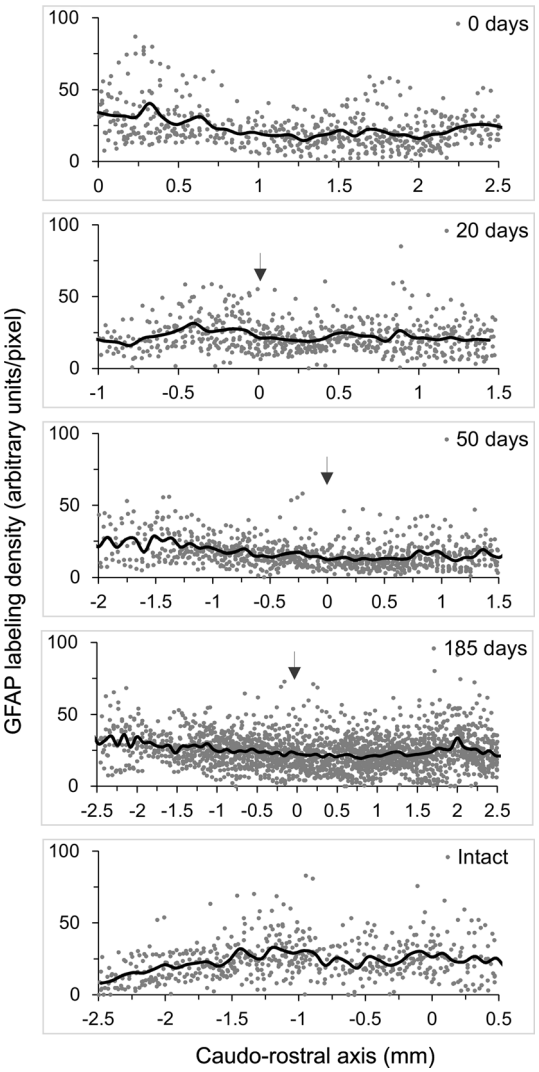


**Fig. 4** Quantification of GFAP immunolabeling in longitudinal sections through the regenerating and intact spinal cord. The average immunolabeling density was determined in longitudinal sections (3–6 sections per time point) subdivided into 50 μm × 50 μm regions of interest (50–562 regions per section). Sections from injured fish were aligned on the caudo-rostral axis such that 0 corresponded to the injury site (*arrows*), whereas sections from intact fish were positioned such that their caudal ends aligned with those of injured fish from the longest survival time group. For statistical analysis, regions of interest were grouped into 200-μm bins (19–127 regions per bin per time point). *Dots* represent the density measurements of individual regions, pooled across fish. Overlaid traces are averages calculated over 80-μm bins

### Two distinct subpopulations of glial cells

To further characterize the glial cell population, tissue sections were immunostained against GFAP and Sox2 in combination with DAPI counterstaining (Fig. 6a–a'''). This experiment was prompted by the observation that part of the glial cells in the cerebellum of *A. leptorhynchus* exhibit stem-cell-like immunological properties (Sîrbulescu et al. 2015). In the present study, the labeling pattern of immunostained cells was examined in intact tissue and at 20 days after amputation, in both non-regenerated and regenerated parts of the spinal cord. A total of 796–1520 cells were analyzed for each of the three conditions: intact, non-regenerated, and regenerated ($n = 3$ sections per condition). Glial cells were classified as either GFAP+/Sox2+ or GFAP+/Sox2− (Fig. 6b). Analysis of the relative numbers of glial cells (normalized to DAPI) revealed a significant difference between the overall proportions of these two subtypes ($F_{(1, 6)} = 41.2$, $p < 0.001$, $\eta^2 = 0.87$), but no effect of experimental condition ($F_{(2, 6)} = 3.25$, $p = 0.11$), nor any interaction between these two factors ($F_{(2, 6)} = 0.90$, $p = 0.46$). Across all three types of spinal cord tissue examined, there were approximately twice as many GFAP+/Sox2− glia (43–55 % of DAPI) than GFAP+/Sox2+ glial cells (22–24 % of DAPI). Overall, 67–78 % of all cells were glia, as identified by GFAP expression, relative to the number of DAPI-stained nuclei. Only 29–36 % of these cells expressed Sox2, indicating that only a fraction of glial cells have stem/progenitor cell potential.

## Discussion

### Absence of gliosis after spinal cord injury

The present study showed no increase in the number or size of GFAP+ or vimentin+ glial cells at the injury site after spinal cord amputation or transection lesions in *A. leptorhynchus*. Similarly, there was no increase in the expression of CSPGs by glial cells located at the injury site, in agreement with previous reports from studies of regenerating zebrafish spinal cord (Becker and Becker 2007). The absence of any significant alteration in the glial network at the location of the injury supports the notion that no glial scar formation occurs after spinal cord lesions in this species. This result is in line with previous reports in other regeneration-competent vertebrates, including chondrichthyans (Kálmán et al. 2013), teleosts (Hui et al. 2010; Baumgart et al. 2012), and urodele amphibians (O'Hara et al. 1992), where no reactive gliosis was observed after CNS injuries.

The present observations are in contrast to the pronounced glial hypertrophy observed after cerebellar stab lesions in *A. leptorhynchus* (Clint and Zupanc 2001). In the corpus cerebelli, one subdivision of the teleostean cerebellum, the density of GFAP+ fibers strongly increased 8 days after the application of the lesion, and remained elevated for at least 100 days after the injury, particularly

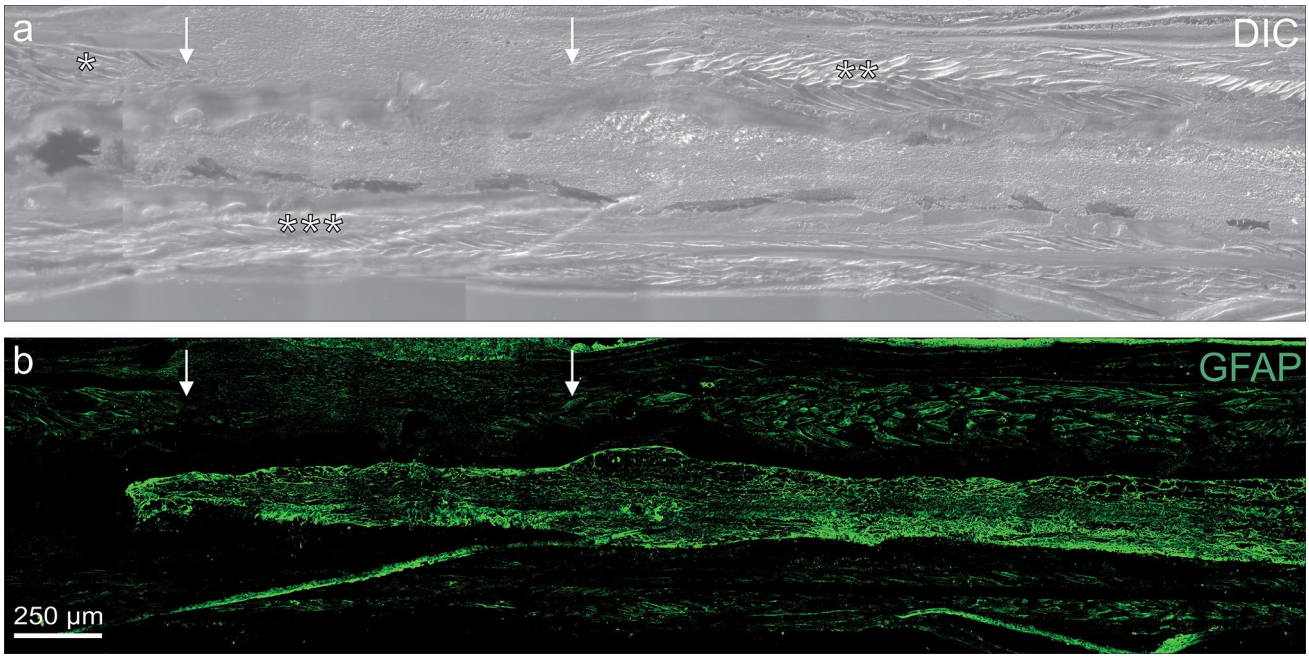


**Fig. 5** Absence of gliosis at the injury site after spinal cord hemisection. **a**, **b** Longitudinal horizontal section through the spinal cord 7 days after the lesion. **a** The differential interference contrast (DIC) image indicates the site of the injury (between the two *arrows*), characterized by the absence of myocytes dextrally to the spinal cord. Differentiated myocytes are clearly evident caudally (*), rostrally (**), and sinistrally (***) to this site. **b** No hypertrophied GFAP-immunopositive glial cells are visible at the injury site. Images are maximum intensity projections of series of 13 0.9-µm-thick confocal optical sections spanning a total of 12.3 µm (**a**), and 16 0.9-µm-thick confocal optical sections spanning a total of 13.5 µm (**b**)

in the molecular layer. The contrasting results between this study and the present investigation may be due to fundamental differences in the cytoarchitecture of the different regions of the CNS, with the intact spinal cord being much richer in GFAP+ glial fibers than the molecular layer of the corpus cerebelli. The astrocytic meshwork induced by lesions in the cerebellum is thought to provide support in the regeneration of the cerebellar tissue, particularly to guide newly generated cells from neurogenic niches to the site of the injury (Clint and Zupanc 2001). It is possible that the spinal cord of *A. leptorhynchus* already contains a sufficiently well-developed glial network that can support regeneration, while in the corpus cerebelli such a network needs to be formed through hypertrophy or cellular proliferation.

### The type of lesion paradigm does not alter the glial response

To examine whether the observed absence of glial scarring in the spinal cord depends on the injury paradigm employed, a hemisection lesion was applied to one fish, and sections through the lesion site were compared with sections obtained after amputation of the caudal portion of the spinal cord. The hemisection paradigm leaves degenerating tissue at the injury site, and might, therefore, elicit a more pronounced glial response. However, no increase in glial immunoreactivity was observed after either type of lesion. This finding confirms that the absence of a glial scar in the spinal cord of *A. leptorhynchus* is independent of the injury paradigm used.

However, this notion does not apply universally to the CNS of regeneration-competent organisms. In the telencephalon of zebrafish, the presence or absence of gliosis depends on the modality through which the injury was induced. Strong glial cell reactivity was observed when a stab wound injury was performed through the skull (März et al. 2011; Kishimoto et al. 2012). By contrast, no glial reaction or scarring was reported after lesioning via the nostrils (Kroehne et al. 2011; Baumgart et al. 2012). After application of the latter lesion paradigm, the injury affects almost half of the telencephalic hemisphere, but does not damage the ventricular zone (where many of the adult stem/progenitor cells of the telencephalon are located) or 'contaminate' the brain parenchyma with other types of tissue or cerebrospinal fluid.

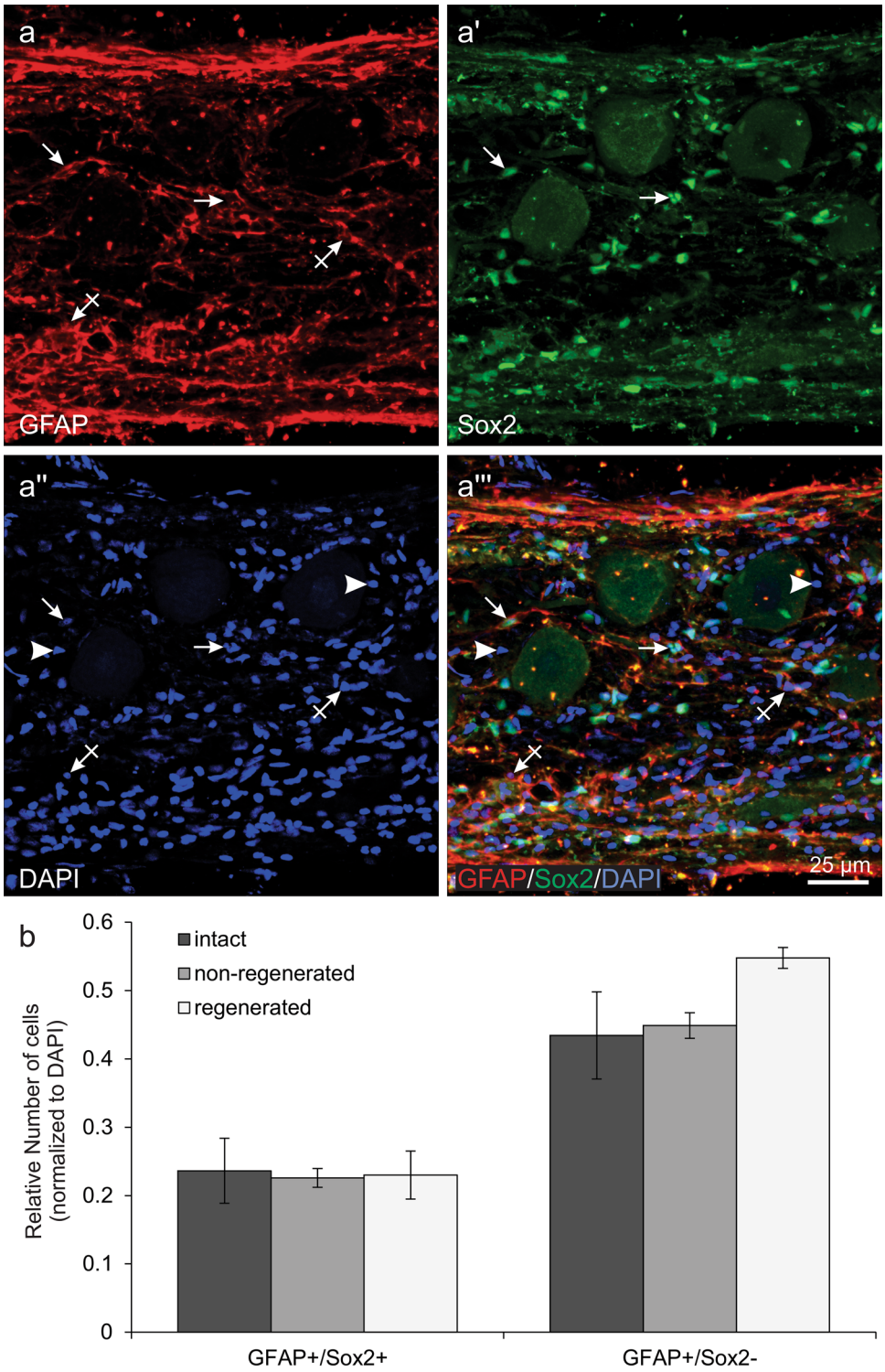


**Fig. 6** Subpopulations of glial cells in the spinal cord. **a**–**a‴** Confocal images illustrating two distinct subtypes of GFAP+ cells in the intact spinal cord. While one of these subpopulations co-expresses Sox2 in the nucleus (*arrows*), the majority of the GFAP-immunopositive glia do not express this stem cell marker (*arrow with cross*). A number of cells shown in the section do not express either GFAP or Sox2 (*arrowheads*). The image represents a maximum intensity projection of a z-stack of 34 1.1-µm-thick confocal optical sections spanning a total of 36.7 µm. **b** Quantitative analysis of the two glial populations in the intact spinal cord, as well as non-regenerated and regenerated parts of the spinal cord at 20 days after amputation (3 sections per condition). No significant differences in the relative numbers of the GFAP+/Sox2+ and GFAP+/Sox2− glial populations were observed between the three experimental conditions. *Error bars* represent SEMs

## The nature of astrocytes is critical for scar formation and central nervous system regeneration

Vertebrates that are able to successfully regenerate after CNS injuries generally share a preponderance of ependymoradial, rather than stellate, parenchymal astrocytes. Interestingly, even in non-regenerating organisms with predominantly ependymoradial glia, such as chelonian reptiles, a similar absence of reactive gliosis has been observed following stab lesions to the telencenphalon

(Kálmán et al. 2013). In *A. leptorhynchus*, like in most teleosts, radial glia represent the only astrocytic cell type observed in the different areas of the brain analyzed thus far (Zupanc et al. 2012; Sîrbulescu et al. 2014, 2015), and likely throughout the entire CNS, including the spinal cord. A well-developed network of glia extends throughout the spinal cord parenchyma, between the central canal and the pial surface, showing a morphology similar to the syncytium described in the pacemaker nucleus located in the brain stem of this species (Sîrbulescu et al. 2014; Zupanc et al. 2014). It is likely that, as demonstrated in other teleosts, glial cells act as a supporting network for the regenerative process, but successful spinal cord regeneration in this system does not necessarily require hypertrophy of existing glia or addition of new glia through cellular proliferation.

## Gliosis as a mechanism of central nervous system regeneration

While the glial scar that forms after CNS injury in mammals has mostly been described as a major inhibitor of axonal regrowth, there are substantial data supporting the beneficial roles of the scar tissue [for review, see (Rolls et al. 2009)]. The glial scar has important functions in the process of healing, by sealing off the injury site, scavenging excess glutamate and potassium ions, providing trophic and metabolic support for the surviving neurons, and even regulating the ensuing immune response. Nevertheless, the production of inhibitory molecules by astrocytes within the glial scar makes this structure a complex barrier to regeneration in mammals (Yiu and He 2006; Fitch and Silver 2008).

By contrast, in most studies of regeneration-competent vertebrates in which gliosis has been reported after CNS injuries, the dense glial network appears to support, rather than inhibit, axonal and neuronal regeneration (Clint and Zupanc 2001; Zupanc and Clint 2003; Hui et al. 2010). Moreover, any glial proliferative or hypertrophic response appears relatively late, often several days after the lesion, when most visible damage to the tissue has already been repaired. In teleost species, it has been reported that GFAP+ glial processes accompany regenerating axons, rather than forming any delimitating scar tissue (Nona and Stafford 1995; Goldshmit et al. 2012; Takeda et al. 2015). A similar phenomenon has been observed in *A. leptorhynchus* during caudal spinal cord regeneration after amputation, where GFAP+ glia appear to accompany the caudal-most axons that grow into the newly formed tissue (RFS, unpublished observations). In the present study, we observed no scar formation or gliosis at the lesion site. These results further endorse the notion that radial glia have a supportive function for axonal and de novo neuronal regeneration in teleost fish and may actively participate in the regenerative process.

## Radial glia as stem/progenitor cells

The experiments in which we employed immunostaining against both GFAP and Sox2 revealed two subpopulations of GFAP+ glial cells: one that co-expresses Sox2, and a second one that lacks immunoreactivity against this stem cell marker. Quantitative analysis has demonstrated that approximately two-thirds of the GFAP+ glia do not express Sox2, whereas the remaining third exhibits such stem-cell-like characteristics. Similar observations, that only part of the GFAP+ glia co-express Sox2, have been made in various brain regions of *A. leptorhynchus* (Sîrbulescu et al. 2014, 2015). The existence of these two subpopulations opens the possibility that they may be differentially affected by trauma. However, the present study shows that SCI does not affect either the size of the GFAP+ glial population or the numbers of its two subpopulations. This finding is remarkable because it not only underscores the notion that no glial scar is formed after injury, but also indicates that the number of radial glia-like stem/progenitor cells does not change after trauma. Since there is a dramatic increase in cell proliferation in response to SCI (Sîrbulescu et al. 2009), we hypothesize that most of the stem/progenitor cells with radial glia-like identity are quiescent in the intact spinal cord and become activated by injury.

## Perspectives

The present study addressed the question of whether a glial scar is formed after amputation and hemisection injuries applied to the spinal cord of *A. leptorhynchus*. Contrary to our expectations, we did not observe any increase in the expression of typical gliosis markers, such as GFAP, vimentin, and CSPGs, at the site of the lesion. We hypothesize that the dense radial glial network already present in the spinal cord of this species acts as a necessary and sufficient supporting system for spontaneous nervous tissue repair. It will be imperative to further investigate in future studies the precise role of radial glia in spinal cord regeneration.

**Acknowledgments** Funding for this investigation was provided by Northeastern University to Günther K.H. Zupanc, and National Science Foundation Grant No. 1538505 awarded to Günther K.H. Zupanc and Rifat Sipahi. All animal experiments were approved by the Institutional Animal Care and Use Committee of Northeastern University. All efforts were made to reduce the number of animals used and to minimize suffering.

## References


Baumgart EV, Barbosa JS, Bally-Cuif L, Götz M, Ninkovic J (2012) Stab wound injury of the zebrafish telencephalon: a model for comparative analysis of reactive gliosis. Glia 60:343–357

Becker CG, Becker T (2007) Zebrafish as a model system for successful spinal cord regeneration. In: Becker CG, Becker T (eds) Model organisms in spinal cord regeneration. Wiley-VCH, Weinheim, pp 289–319

Becker T, Wullimann MF, Becker CG, Bernhardt RR, Schachner M (1997) Axonal regrowth after spinal cord transection in adult zebrafish. J Comp Neurol 377:577–595

Bernstein JJ, Bernstein ME (1969) Ultrastructure of normal regeneration and loss of regenerative capacity following teflon blockage in goldfish spinal cord. Exp Neurol 24:538–557

Clint SC, Zupanc GKH (2001) Neuronal regeneration in the cerebellum of adult teleost fish, *Apteronotus leptorhynchus*: guidance of migrating young cells by radial glia. Dev Brain Res 130:15–23

Cregg JM, DePaul MA, Filous AR, Lang BT, Tran A, Silver J (2014) Functional regeneration beyond the glial scar. Exp Neurol 253:197–207

Diaz Quiroz JF, Echeverri K (2013) Spinal cord regeneration: where fish, frogs and salamanders lead the way, can we follow? Biochem J 451:353–364

Dusart I, Schwab ME (1994) Secondary cell death and the inflammatory reaction after dorsal hemisection of the rat spinal cord. Eur J Neurosci 6:712–724

Fitch MT, Silver J (2008) CNS injury, glial scars, and inflammation: inhibitory extracellular matrices and regeneration failure. Exp Neurol 209:294–301

Fitch MT, Doller C, Combs CK, Landreth GE, Silver J (1999) Cellular and molecular mechanisms of glial scarring and progressive cavitation: in vivo and in vitro analysis of inflammation-induced secondary injury after central nervous system trauma. J Neurosci 19:8182–8198

Goldshmit Y, Sztal TE, Jusuf PR, Hall TE, Nguyen-Chi M, Currie PD (2012) Fgf-dependent glial cell bridges facilitate spinal cord regeneration in zebrafish. J Neurosci 32:7477–7492

Horn KP, Busch SA, Hawthorne AL, van Rooijen N, Silver J (2008) Another barrier to regeneration in the central nervous system: activated macrophages induce extensive retraction of dystrophic axons through direct physical interactions. J Neurosci 28:9330–9341

Hui SP, Dutta A, Ghosh S (2010) Cellular response after crush injury in adult zebrafish spinal cord. Dev Dyn 239:2962–2979

Kálmán M, Somiya H, Lazarevic L, Milosevic I, Ari C, Majorossy K (2013) Absence of post-lesion reactive gliosis in elasmobranchs and turtles and its bearing on the evolution of astroglia. J Exp Zool B 320:351–367

Kishimoto N, Shimizu K, Sawamoto K (2012) Neuronal regeneration in a zebrafish model of adult brain injury. Dis Model Mech 5:200–209

Kroehne V, Freudenreich D, Hans S, Kaslin J, Brand M (2011) Regeneration of the adult zebrafish brain from neurogenic radial glia-type progenitors. Development 138:4831–4841

Kwon BK, Tetzlaff W, Grauer JN, Beiner J, Vaccaro AR (2004) Pathophysiology and pharmacologic treatment of acute spinal cord injury. Spine J 4:451–464

Lee-Liu D, Edwards-Faret G, Tapia VS, Larraín J (2013) Spinal cord regeneration: lessons for mammals from non-mammalian vertebrates. Genesis 51:529–544

März M, Schmidt R, Rastegar S, Strähle U (2011) Regenerative response following stab injury in the adult zebrafish telencephalon. Dev Dyn 240:2221–2231

Nona SN, Stafford CA (1995) Glial repair at the lesion site in regenerating goldfish spinal cord: an immunohistochemical study using species-specific antibodies. J Neurosci Res 42:350–356

O'Hara CM, Egar MW, Chernoff EAG (1992) Reorganization of the ependyma during axolotl spinal cord regeneration: changes in intermediate filament and fibronectin expression. Dev Dyn 193:103–115

Reimer MM, Sörensen I, Kuscha V, Frank RE, Liu C, Becker CG, Becker T (2008) Motor neuron regeneration in adult zebrafish. J Neurosci 28:8510–8516

Rolls A, Shechter R, Schwartz M (2009) The bright side of the glial scar in central nervous system repair. Nat Rev Neurosci 10:235–241

Sîrbulescu RF, Zupanc GKH (2011) Spinal cord repair in regeneration-competent vertebrates: adult teleost fish as a model system. Brain Res Rev 67:73–93

Sîrbulescu RF, Zupanc GKH (2013) Neuronal regeneration. In: Evans DH, Claiborne JB, Currie S (eds) The physiology of fishes. CRC Press, Boca Raton, pp 405–441

Sîrbulescu RF, Ilieş I, Zupanc GKH (2009) Structural and functional regeneration after spinal cord injury in the weakly electric teleost fish, *Apteronotus leptorhynchus*. J Comp Physiol A 195:699–714

Sîrbulescu RF, Ilieş I, Zupanc GKH (2014) Quantitative analysis reveals dominance of gliogenesis over neurogenesis in an adult brainstem oscillator. Dev Neurobiol 74:934–952

Sîrbulescu RF, Ilieş I, Vitalo AG, Trull K, Zhu J, Traniello IM, Zupanc GKH (2015) Adult stem cells in the knifefish cerebellum. Dev Neurobiol 75:39–65

Sofroniew MV, Vinters HV (2010) Astrocytes: biology and pathology. Acta Neuropathol 119:7–35

Takeda A, Goris RC, Funakoshi K (2007) Regeneration of descending projections to the spinal motor neurons after spinal hemisection in the goldfish. Brain Res 1155:17–23

Takeda A, Atobe Y, Kadota T, Goris RC, Funakoshi K (2015) Axonal regeneration through the fibrous scar in lesioned goldfish spinal cord. Neuroscience 284:134–152

Traniello IM, Sîrbulescu RF, Ilieş I, Zupanc GKH (2014) Age-related changes in stem cell dynamics, neurogenesis, apoptosis, and gliosis in the adult brain: a novel teleost fish model of negligible senescence. Dev Neurobiol 74:514–530

Yiu G, He Z (2006) Glial inhibition of central nervous system axon regeneration. Nat Rev Neurosci 7:617–627

Yuan YM, He C (2013) The glial scar in spinal cord injury and repair. Neurosci Bull 29:421–435

Zupanc GKH, Clint SC (2003) Potential role of radial glia in adult neurogenesis of teleost fish. Glia 43:77–86

Zupanc GKH, Sîrbulescu RF (2013) Teleost fish as a model system to study successful regeneration of the central nervous system. Curr Top Microbiol Immunol 367:193–233

Zupanc GKH, Sîrbulescu RF, Ilieş I (2012) Radial glia in the cerebellum of adult teleost fish: implications for the guidance of migrating new neurons. Neuroscience 210:416–430

Zupanc GKH, Ilieş I, Sîrbulescu RF, Zupanc MM (2014) Large-scale identification of proteins involved in the development of a sexually dimorphic behavior. J Neurophysiol 111:1646–1654